Many-particle simulation of Rydberg exciton interaction

Florian Morawetz* and Stefan Scheel
Institut für Physik, Universität Rostock, Albert-Einstein-Straße 23, D-18059 Rostock, Germany

Julian Heckötter and Marc Aßmann
Experimentelle Physik 2, Technische Universität Dortmund, D-44221 Dortmund, Germany

(Received 1 September 2023; revised 3 November 2023; accepted 14 November 2023; published 14 December 2023)

Rydberg physics, with its characteristic long-range interactions between single quantum states, was introduced into semiconductor physics with the observation of Rydberg excitons. To identify and understand spectroscopic signatures of those long-range interactions, we propose a quantitative simulation of an ensemble of Rydberg excitons. By reproducing typical pump-probe absorption spectra, we discuss the influence of the assumed van-der-Waals-type interaction potentials.

DOI: 10.1103/PhysRevB.108.235205

I. INTRODUCTION

With the rapidly evolving techniques of trapping and controlling single atoms, Rydberg systems matured into a leading field for quantum simulation and quantum computation [1,2]. The exaggerated van der Waals (vdW) interactions between Rydberg states mediate hereby a coherent evolution of atoms which themselves can be macroscopic distances apart.

Rydberg excitons may provide the corresponding semiconductor implementation which holds the promise of presenting a robust and more scalable system. The material cuprous oxide (Cu_2O), in which excitonic Rydberg physics was investigated [3], has seen a resurgence of interest in the past decade [4–8], and proposals for coherent schemes [9,10] and applications in nonlinear quantum optics with exciton-polaritons [11] have recently been put forward. While excited excitons were also observed in monolayer transition-metal dichalcogenides such as WSe_2 [12], Cu_2O is regarded as the most suitable material for the exploitation of long-range interexcitonic interactions, as only there large quantum numbers of up to $n = 30$ can be resolved [13]. This extraordinary property is related to the equal parity of the lowest conduction and highest valence bands, which leads to a dominant (optical dipole) excitation of p-type excitons in the so-called yellow series. We will focus our attention on excitons of this type, although Cu_2O is known to possess a rich band structure [14] with several excitonic series, which may serve as an additional resource [15].

The inherent properties of the semiconductor system, however, pose additional challenges for the investigation of the interaction between Rydberg states. It was recognized [16] that the influence of an inevitable micro-plasma, which is induced concomitantly with the (optical) creation of excitons, can lead to similar effects as the vdW interaction between Rydberg excitons. In typical continuous wave (cw) experiments, it is not always possible to differentiate between those two mechanisms [17], both of which we will review briefly in Sec. II.

Light was shed on this issue by utilizing a pump-probe setup [18] to effectively decouple the strength of the blockade (controlled via the pump power) from the type of the blockaded exciton (controlled via the probe frequency). The remarkable agreement of characteristic features in the differential spectra with a corresponding theoretical model, which employed only a pairwise vdW-type interaction potential, gave more arguments in favor of exciton-exciton interactions as the dominant factor in these experiments. However, fine details of the experimental absorption spectra could not be explained by the theoretical modeling. The question thus remained whether those deviations can be attributed to the employed approximations or whether indeed other influences, such as the mentioned microplasma, have a larger impact.

To clarify this point more, we suggest an alternative numerical simulation of the absorption spectra, based on a microscopic distribution of pump excitons. The aim of our simulation is to provide a more quantitative modeling of the absorption spectra, consistent with crystal thicknesses of several tenths of micrometers as in typical experiments. By considering different interaction channels between the np-type excitons as well as the averaged influence of charged impurities, we will attempt to explain the experimental spectra in more detail. To that end, we briefly sketch the pump-probe experiment in Sec. III, whose outcomes we aim to simulate. The exciton-exciton interaction in Sec. II B is the basis for our simulation, which we explain in detail in Sec. IV. After presenting the results of our simulation in Sec. V, we discuss the outcomes in detail in Sec. VI, before providing an outlook on further applications in a final conclusion in Sec. VII.

II. INTERACTIONS BETWEEN RYDBERG EXCITONS

An observed power-dependent bleaching [17] of the excitonic resonances can be attributed either to pump-induced changes in the crystal environment [16] or to interactions between Rydberg excitons [3]. While the latter effect can be described akin to atomic physics, the former effect is truly a semiconductor specific feature which is caused by the creation

*florian.morawetz@uni-rostock.de

of a microplasma. In the following, we review these two mechanisms out of which we implemented only the exciton-exciton interaction in our simulation.

A. Plasma effect

It is well established [19] that, for sufficiently high densities of excitons (when the carrier separation becomes comparable with the Bohr radius), a Mott transition from an excitonic phase to a so-called electron-hole plasma (EHP) occurs in semiconductors. This transition can also be reached by directly creating electrons and holes in the system by optical pumping above the band gap. The free carriers in the semiconductor induce a renormalization and thus lowering of the band gap, whereas the positions of the excitonic resonances do not shift as the reduction of the exciton binding energy introduced by the plasma cancels the band gap reduction almost exactly. The Rydberg exciton resonances bleach successively with increasing pump power when the renormalized band gap crosses their resonance energy. This effect must be considered when pumping below the band gap, as also via exciton relaxation as well as Auger scattering [20], an EHP can be created [21].

B. Exciton-exciton interaction

The interaction potentials between two Rydberg excitons in Cu_2O have been calculated [22] in analogy to atomic systems [23], out of which we summarize here the main steps. The expansion of the mutual Coulomb interactions between the electrons and holes of two excitons into a multipole series can be truncated after the first term. Neglecting the terms beyond the dipole-dipole interaction is well justified under the assumption that the distance R between the excitons is much larger than their size, which can be quantified via the LeRoy radius:

$$R \gg R_{\mathrm{LeRoy}} = 2\left(\sqrt{\langle r_1^2\rangle} + \sqrt{\langle r_2^2\rangle}\right), \tag{1}$$

where r_1 and r_2 are the relative coordinates corresponding to the individual excitons. Under this condition, exchange effects can be neglected. The two-exciton Hamiltonian with an interaction term:

$$V^{1,2} = \frac{e^2}{4\pi\epsilon_0\epsilon_r}\left[\frac{\mathbf{r}_1\cdot\mathbf{r}_2}{R^3} - \frac{3(\mathbf{r}_1\cdot\mathbf{R})(\mathbf{r}_1\cdot\mathbf{R})}{R^5}\right], \tag{2}$$

can then be diagonalized in a basis of product states of two single-exciton states [24].

For large R, the deviation of the two-exciton energies from the sum of their single-exciton energies can also be calculated in perturbation theory. The resulting potential curves follow a vdW- type interaction law $\propto\frac{C_6}{R^6}$. The C_6 coefficients scale as $\propto n^{11}$ and are used as input parameters for our simulation. This interaction leads to the Rydberg blockade phenomenon [25], where a Rydberg state impedes the creation of a second one in its vicinity. This is the case when the mutual vdW interaction shifts the second Rydberg state out of resonance, which leads to smaller absorption from a resonant laser and thus to a decreased oscillator strength which deviates [3] from the expected scaling with $\propto n^{-3}$.

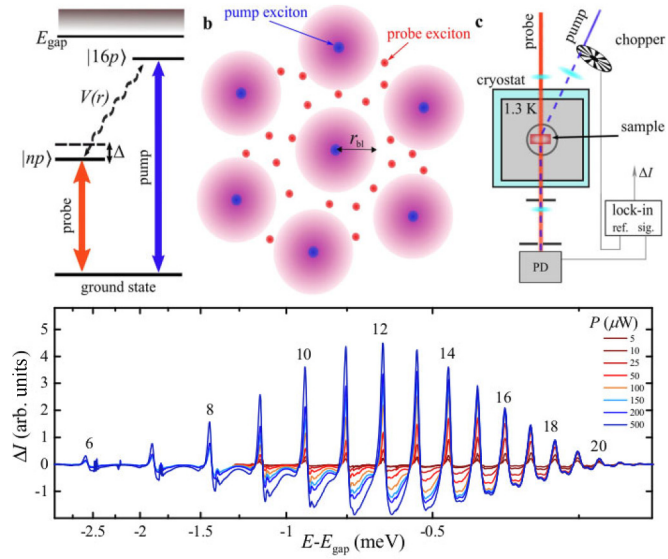

FIG. 1. Schematic experimental setup (top) and characteristic differential absorption spectra (bottom) for a fixed pump laser at $n = 16$: Our simulation aims at reproducing and understanding the observed spectra via a vdW-type interaction mechanism; figure adapted from Ref. [18].

III. PUMP-PROBE EXPERIMENT

A further in-depth study of the interactions of Rydberg excitons was published recently [18] using a natural Cu_2O sample held at 1.3 K. Here, the crystal was excited with two stabilized dye lasers, which served different purposes: The pump laser at 570.9014 nm created a distribution of excitons whose density depends on the laser power, while the absorption spectrum of the probe laser was measured simultaneously. The probe laser had a high spectral resolution of 5 neV as well as a tunability range from 620 to 565 nm which covers all excitonic resonances. By using a low-frequency modulation of the pump laser with an optical chopper, the slightest pump-induced changes in the differential absorption spectrum could be detected via a lock-in amplifier. This allowed us to use low laser powers (compared with previous works [16]), which reduced the role of possible plasma effects. Measured characteristic differential absorption spectra can be seen in Fig. 1, which shows a pump-induced decrease at the excitonic resonances as well as an increase of the absorption for a blue-detuned probe laser. While the former has been interpreted as the Rydberg blockade induced by the pump excitons, the latter could accordingly indicate a facilitation mechanism [17], where the interaction between pump and probe excitons compensates the detuning and thus leads to an increased probe laser absorption. Further fine details of those spectra, such as the occurrence of an isosbestic point at the blue-detuned side of all resonances, could only be explained by using an underlying (vdW) power-law interaction potential. The origin of other details, however, such as facilitation features for red-detuned probe frequencies, could not be unambiguously explained.

However, most importantly, the pump power and thus the blockaded volume can be varied independently from the probe frequency in this type of experiment. By measuring

the increase of the blockade (i.e., maximal transmission) with the pump power for all excitonic resonances, one can deduce the relative strength of the underlying asymmetric vdW interaction between the (pump) $n'p$ and (probe) np excitons by means of the respective C_6 coefficients. It is shown that those interaction coefficients scale approximately with

$$C_6(n, n') \propto \frac{n^4 (n')^4}{n^{-3} + (n')^{-3}}, \tag{3}$$

where in the experiment, the pump frequency is fixed to $n' = 16$. This type of scaling was derived from a vdW-type interaction law, where the dipole matrix elements of the interacting excitons, which scale as $\propto n^2$, contribute quadratically, while the Förster defect scales as $\propto n^{-3}$ and enters the denominator.

Although such a scaling law ignores possible Förster resonances, we use it in our simulation to estimate the strength of the asymmetric Rydberg blockade in combination with the calculated absolute (symmetric) interaction strengths [22]. In this way, one can directly observe which of the features in the experimental spectra can be reproduced and explained solely on the basis of a vdW-type exciton-exciton interaction mechanism.

We aim at simulating only the low-power regime of the experiment where the density of a pump-induced EHP is lower than the Mott density for all investigated excitons (see Appendix A).

IV. SETUP OF THE SIMULATION

Our simulation is based on the assumption that changes in the absorption of the probe laser are induced by a fixed distribution of pump excitons. We use this static picture to simulate typical cw experiments in which a balancing of simultaneous creation and decay of pump and probe excitons leads to a steady-state absorption. The assumption to treat the excitons as stationary is well justified as the exciton traversal time of $\approx$10 ns across the crystal is several orders of magnitude larger than their lifetime. The two steps of the simulation, i.e., the generation of a correlated distribution of pump excitons as well as the calculation of the resulting absorption spectra, are explained in detail in the following. The underlying idea for both steps is hereby that the energy needed to create a second exciton within the vicinity of another is increased by the interaction energy between the two excitons. This shifts the exciting laser out of resonance (blockade effect) or into the resonance if it is initially detuned (facilitation).

A. Distribution of pump excitons

We chose a sequential setting of a fixed number N of $16p$-pump excitons (on-resonance excitation). Different exciton densities can then be mapped to different pump powers (or vice versa) based on the blockade efficiency [3] (see Appendix A). While the position of the first pump exciton is random, the next one has a reduced probability to be excited in the vicinity of the first, as the mutual vdW interaction leads to a shift Δ_{vdW} out of the resonance. The decreased probability is estimated via the height of the resonance peak at this detuning:

$$P = \frac{1}{1 + \left(\frac{2}{\Gamma_{16}} \Delta_{\mathrm{vdW}}\right)^2}, \tag{4}$$

where the parameter Γ_{16} is the corresponding line width of the $16p$-exciton resonance. Each added exciton alters this probability distribution, based on which the position of the next exciton is chosen. This procedure leads to a distribution of vdW-correlated pump excitons. This first part of our simulation thus amounts to a more sophisticated version of previous Monte Carlo simulations [26] to estimate the influence of the blockade effect.

Although this type of setting seems similar to simulations of the evolution of Rydberg populations [27], it is not possible to do the same type of analysis in the present case. The setting of excitons in our simulation serves only as a tool to generate a final distribution and should not be mistaken for the dynamics of the excitonic system, which would be more involved.

B. Calculation of probe absorption

For sufficiently low probe powers, we can neglect the interaction between probe excitons. Then only the vdW interaction with the pump excitons leads to a shift of the (probe) exciton energies. More specifically, based on the positions of the pump excitons, we calculate a position-dependent probability distribution for exciting a probe exciton, analogous to Eq. (4). In contrast to the previous subsection, the frequency of the exciting laser ω_{probe} is no longer fixed but must be scanned over all excitonic resonances to calculate an absorption spectrum. This necessitates several refinements: (1) The detuning Δ_{vdW} is replaced by the overall detuning $\tilde{\omega}_n = \omega_n - \Delta_{\mathrm{vdW}} - \omega_{\mathrm{probe}}$ from the excitonic resonance frequency ω_n. (2) The resonance peaks can be described by asymmetric Lorentzians [28] which are characterized by the oscillator strength O_n and an additional asymmetry parameter q_n that quantifies the asymmetry of the resonance peak; $q_n = 0$ corresponds to a symmetric Lorentzian. (3) The vdW shift, linewidth, oscillator strength, and the asymmetry parameter depend on the type of exciton (np) which is excited. For a resonant probe laser ($\omega_{\mathrm{probe}} = \omega_n$) and well-isolated resonances ($\omega_n - \omega_{n-1} \gg \Gamma_n$), it is sufficient to consider the absorption into only one type of exciton. Then again, for highly excited Rydberg states and for strongly detuned probe frequencies, different np excitons significantly contribute to the overall absorption probability. Therefore, the overall absorption is obtained from a sum over the contributions from all excitonic resonances and a subsequent integration over the spatial probability distribution (see Fig. 2) according to

$$\alpha(\omega_{\mathrm{probe}}) = \int_V \sum_n \frac{O_n}{\pi} \frac{\Gamma_n/2 + 2q_n\tilde{\omega}_n(\mathbf{r})}{(\Gamma_n/2)^2 + [\tilde{\omega}_n(\mathbf{r})]^2} \mathrm{d}^3\mathbf{r}. \tag{5}$$

1. Choice of parameters Γ_n, O_n, q_n

The linewidths Γ_N, oscillator strengths O_n, and the asymmetry parameters q_n of the excitonic resonances are essential parameters in our simulation. The first two are expected to scale as $\propto \frac{n^2-1}{n^5}$ with the principal quantum number [29].

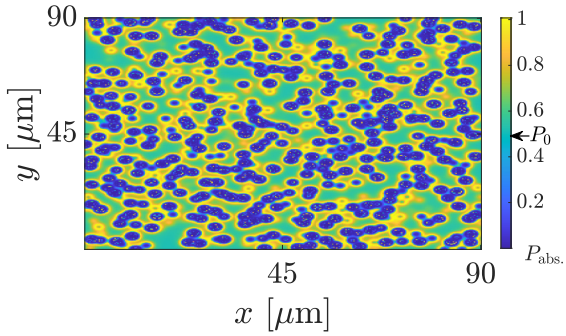

FIG. 2. Probability distribution for exciting a probe exciton in a distribution of $N = 3000$ pump excitons normalized to the absorption probability under resonant excitation ($n = 15$); here, blue detuned probe excitation leads to a smaller absorption probability (P_0) without the influence of the pump excitons (background); interaction with the pump excitons leads to blockaded areas (blue discs) and regions where the excitation is facilitated (yellow circles); P_{abs} refers to Eq. (5) before spatial integration.

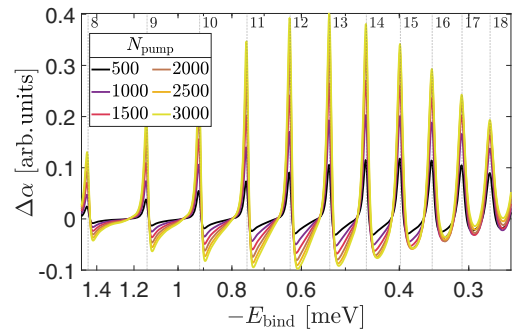

FIG. 3. Simulated differential absorption spectrum for different numbers of pump excitons N in a volume of $60\times60\times10\,\mu\text{m}^3$.

However, a substantial deviation from those scaling laws was measured for both quantities [3]. While in Ref. [3] a bleaching of the oscillator strengths has been assigned to the Rydberg blockade effect, an additional broadening of the lines could be partly attributed to the influence of charged impurities in the crystal [30]. Those are inevitable in real crystals (up to now, the qualitatively purest crystals are still natural ones [5]), and their effect was simulated by using a Holtsmark distribution to model the resulting microfield in the crystal and calculating the corresponding Stark states. From the resulting spectrum, new effective parameters Γ_n, O_n, q_n were obtained, which demonstrate for increasing n an additional broadening, a reduction of the oscillator strength as well as a change in the asymmetry parameters. We take those parameters [30] from an assumed impurity concentration of $1.2\times10^9\,\text{cm}^{-3}$ as input into our simulation, where for the investigated quantum numbers ($n < 19$), the scaling of the oscillator strengths still resembles the ideal scaling. We expect to reproduce the experimentally observed reduction of the oscillator strengths from our simulation of the Rydberg-Rydberg interaction. The impurities induce an inhomogeneous broadening of the lines, such that the linewidths Γ_n no longer follow the ideal n^{-3} scaling.

2. Anisotropic interaction

As a further refinement, we also consider the fixed polarization of the exciting lasers. As the employed exciton-exciton interaction conserves the overall magnetic quantum number $M = m_1 + m_2$, the excitonic pair states ψ_{M_i} are labeled with respect to it [22]. The projection of some M state (on the interexcitonic axis) onto the polarization state of the lasers (i.e., the laser would excite the exciton in the laboratory frame) determines the probability to excite the corresponding M state via the overlap $O = |{}_{\text{lab}}\langle nlm, n'l'm'\,|\psi_{M_i}\rangle_{\text{mol.}}|^2$. The overlap can be calculated by transforming the product state $|nlm, n'l'm'\rangle_{\text{lab}}$ to the molecular frame (defined by the interexcitonic axis) using the Wigner D matrix [31], see Appendix B. Each M state has a different C_6 coefficient which varies in strength as well as sign and leads to a different vdW shift and absorption strength. Therefore, we consider those different interaction channels by calculating the probe absorption for each M state and average over them, weighted with the probability that the corresponding state was in fact excited. With this procedure, the effective absorption becomes dependent on the laser polarizations and the relative positions of pump and probe excitons, which mimics an underlying anisotropic interaction. For such a procedure, however, we consider only the interaction with the closest pump exciton at each position, as a certain M state can only be defined for a pairwise exciton-exciton interaction. Although schemes for the calculation of interaction potentials between three particles were proposed for atomic Rydberg systems [32], such a treatment goes beyond the scope of this paper.

V. RESULTS

In this section, we present and analyze the results of our simulation of the probe spectra. The obtained differential spectra, i.e., the difference of the transmission spectra in the presence and absence of pump excitons, can be seen in Fig. 3 for different numbers N of pump excitons. Our model enables us to reproduce the blockade and facilitation features of the experiment [18] as well as the increase of the blockade strength with the number of pump excitons. Note that, to obtain the n-dependent increasing and decreasing (tentlike) behavior of the differential blockade peaks, we need to include the actual linewidths which deviate from the ideal scaling law ($\propto n^{-3}$). Approximately, one also obtains an isosbestic point which, however, is blurred for large numbers of pump excitons, in agreement with experiments at larger pump powers.

The most apparent differences to the experiment are the relatively narrow width of the facilitation features compared with the broader ones from the experiment as well as the absence of facilitation features at the red-detuned side of the resonances. Although in our simulation we average over attractive and repulsive vdW potentials, the results do not show the expected increase of absorption for a red-detuned laser due to attractive exciton-exciton interactions (facilitation) in the differential absorption spectra. This discrepancy can be explained by the fact that the repulsive C_6 coefficients as well as the overlaps of the corresponding M states are larger than the attractive ones. This leads to a negligible influence of the contributions with increased absorption for a red-detuned probe laser during

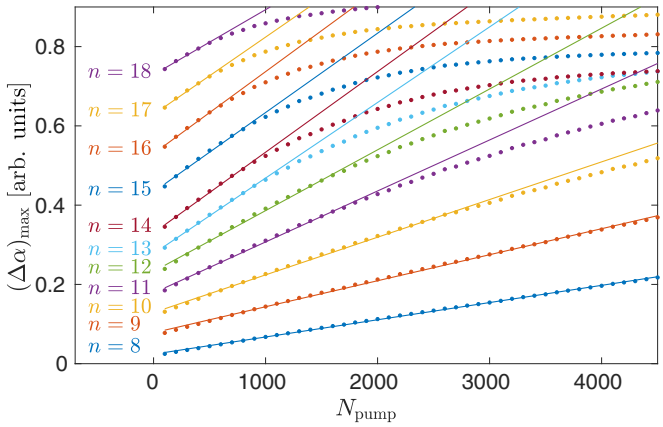

FIG. 4. Maximal differential absorption in dependence on the pump exciton number ($\propto$ pump power) at the different probe exciton resonances n. Lines are shifted vertically for better visibility, compare with Fig. 2 in the supplement of Ref. [18]: An initial linear increase saturates, which corresponds to a complete bleaching of the excitonic resonance.

the averaging process. Why the experiment nonetheless shows an increased absorption at those frequencies will be discussed shortly.

The peak heights of the differential absorption (maximal blockade strength) saturate. We observe the onset of this saturation at smaller pump strengths for larger n (see Fig. 4). Such a behavior was attributed to the stronger vdW interactions between the highly excited states, which leads to a larger crystal volume being blocked for probe absorption by one pump exciton and thus to a fully blockaded crystal volume (i.e., no probe excitons are excited) already at lower pump powers. By using the approximate measure of the blockade radius $R_{\text{bl}}(n) = \sqrt[6]{C_6(16, n)/\Gamma_n}$ as the minimal distance from a pump exciton at which a probe exciton can be created, we see that saturation sets in when the volume filled by spheres with radius R_{bl} is ∼10–40% of the total volume. When mapping the exciton density to the pump power (as described in Appendix A), we identify the onset of the saturation at similar powers as in the experiment, which quantitatively confirms our simulation. Furthermore, we reproduce the experimentally measured behavior, which shows that the blockade strength of excitons with smaller n increases linearly, while the blockade strength of the larger excitons is already saturated.

Finally, our simulation provides a prediction for the probability to excite a probe exciton at a certain distance away from the nearest pump exciton. By plotting the full distribution for all distances, we can analyze and predict the occurring spatial correlations between pump and probe excitons for different probe frequencies. To obtain this distribution, we sum up the weights at all positions that have the same distance to the nearest pump exciton and plot this cumulative weight as a function of the occurring distances (see Fig. 5). For resonant probe excitation (upper panel) $\omega_{\text{probe}} = \omega_{10}$, the Rydberg blockade leads to a suppression of small distances such that the obtained distribution resembles the packing of a given number of hard (blockaded) spheres in a fixed volume. In contrast, for a blue-detuned probe laser ($\omega_{\text{probe}} > \omega_{10}$), we observe a more peaked structure, where the probe excitons are predominantly created

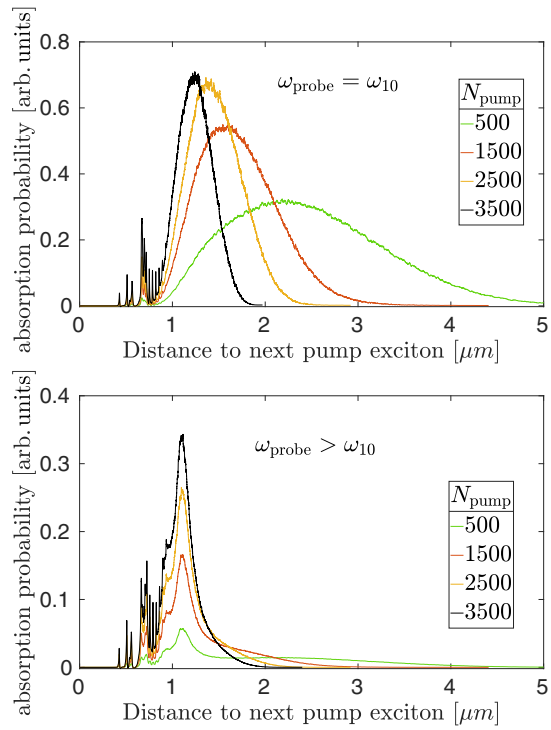

FIG. 5. Simulated expected distribution of distances between pump and probe excitons; a resonant probe laser induces a distribution as expected for hard spheres, while a blue detuned probe laser leads to the appearance of pronounced preferred pump-probe distances.

at a fixed distance from the pump excitons. At this distance, the vdW shift compensates the initial detuning, which leads to the given correlated distribution of pump and probe excitons through a facilitated excitation.

In both cases, we obtain additional small peaks at short distances that originate from states with quantum number $n \neq 10$, whose excitation is facilitated for very small pump-probe distances. Those small distances are, however, not covered with our initial assumptions ($R \ll R_{LR}$); hence, we consider those peaks as artifacts from the simulation. While it is not clear whether the probe excitation in the direct vicinity of the pump excitons is suppressed completely, the calculation of corresponding excitonic pair states would require (at least) higher orders in the multipole expansion.

VI. DISCUSSION

Our modeling includes solely pairwise (vdW) power-law Rydberg-Rydberg interactions to simulate the main outcomes of pump-probe experiments. With this neglect of the influence of the plasma, we succeeded in reproducing the main features of the experimental spectra, as can be seen in the results.

The quantitative agreement of our simulation with the experiment is especially remarkable in the respect that the employed perturbative (vdW) interaction potentials were only derived for large interexcitonic distances (with respect to LeRoy radius). In contrast to atomic systems, where a low atomic density or even fixed positions of the atoms in tweezer arrays can rule out small distances [33], this is neither in

the experiment nor in the simulation strictly ensured for an excitonic system (note that, due to the composite nature of excitons, the interactions become even more complex for small distances than for the atomic case [34]). However, the successful modeling of the experiment insinuates the sufficiency of using only the dipole-dipole interaction potentials in the simulation (for all interexcitonic distances). This can be reasoned by the assumption that the crystal volume with positions which are very close to pump excitons, only gives rise to a negligible contribution to the overall probe absorption when performing the spatial averaging over a distribution of pump excitons.

Since we are investigating a complex system within a semiconductor environment, it is not surprising that minor experimentally observed features, such as the appearance of facilitation features on the red-detuned side of the excitonic resonances, were not reproduced by the simulation. Those could possibly arise from changes of the interaction potentials by, e.g., impurity-induced microfields (for atomic systems the influence of electric fields on Rydberg-Rydberg interactions is evaluated with tools such as the software PAIRINTERACTION [23]), Förster resonances in the asymmetric vdW interactions, or interactions with excitons of higher angular quantum numbers [35]. While the relative importance of those refinements is hard to estimate *a priori* and an inclusion of all possible influences is numerically not possible, the underlying idea of dominant Rydberg-Rydberg interactions would not change when adding more corrections. Vice versa, our simulation apparently includes the most important effects as it reproduces the main features of the differential spectra, such as nonshifting blockade maxima and facilitation minima as well as an (quantum number-dependent) increase and saturation of the blockade strength with pump power. Based on the successful modeling of all these features, it seems reasonable to retain the interpretation of the vdW interaction as being the dominant interaction.

VII. CONCLUSIONS

In this paper, we have simulated the change in differential pump-probe spectra due to a vdW interaction between pump and probe excitons. By reproducing the main features of experimental spectra, we provide more evidence for the dominance of the interexcitonic vdW interaction. Compared with solving the equations of motion for products of exciton operators by a hierarchical expansion [18,36], our direct numerical approach allows us to model the extended spatial distribution of excitons for typical pump probe setups. The strong impact of the angle between interexcitonic (molecular) axis and laser axis on the interaction potentials [6] was explicitly included in the spatial averaging for the calculation of the absorption spectra, yielding a quantitative modeling of current experiments.

This approach resulted in a remarkable agreement between simulation and experiment [18]. However, qualitative differences in the spectra remained, even when including the average influence of impurities in our model. In this regard, a more rigorous calculation of the pair potentials, especially in the presence of charged impurities, seems worthwhile to exclude or underline the need for alternative explanations.

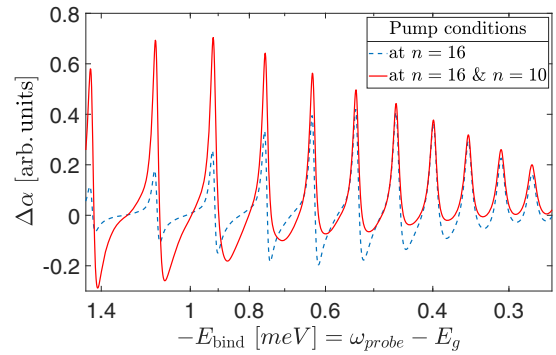

FIG. 6. The height of the differential absorption peaks (blockade strength) can be further increased by using a secondary pump laser which creates excitons of smaller size. Here, creation of $N = 4000$ $16p$-type excitons and $N = 80000$ $10p$-type excitons.

Most importantly, the presented simulation enables us to predict ideal conditions for pump-probe experiments to achieve optimal blockade effects. For example, we propose using a combination of two pump lasers, resulting in an optimized filling of the crystal volume. Accordingly, one reaches stronger maximal blockade strengths also for intermediate exciton sizes ($n_{\rm probe} = 8$–12), as shown in Fig. 6.

While the narrow cw laser bandwidth has been neglected in our simulation, it can and must be included for the modeling of experiments using pulsed lasers. In this way, our model can also be directly adapted to investigate the influence of the vdW interaction strength in time-resolved experiments, such as in recent studies in which s excitons are excited via second harmonic generation [37].

ACKNOWLEDGMENT

This paper was financially supported by the Deutsche Forschungsgemeinschaft through SPP 1929 GiRyd (SCHE 612/4-2). We thank Prof. H. Stolz for useful discussions.

APPENDIX A: RELATION BETWEEN LASER POWER AND EXCITON DENSITY

We propose a mapping between laser power and generated exciton density that is based on basic scaling arguments [3]. The exciton density ρ scales with the absorption strength α times the laser power P_L, which is deposited within the exciton lifetime Γ_n; hence, $\rho \propto P_L\alpha/\Gamma_n$. Vice versa, the absorption is reduced with increased exciton density $\alpha = \alpha_0(1 - \rho V_{\rm bl})$, and thus, we find the scaling law for the dependence of ρ on laser power as

$$\rho = \frac{1}{V_{\rm bl}^n[1 + (S_n P_L)^{-1}]}. \tag{A1}$$

The blockade efficiency S_n has been determined experimentally [3] and is estimated as $S_{16} = 1.3\,{\rm mW}^{-1}$ for the $16p$ exciton. The blockade volume is defined as $V_{\rm bl}^n = \frac{4}{3}\pi(R_{\rm bl}^n/2)^3$ with the blockade radius $R_{\rm bl}^n = \sqrt[6]{\frac{C_6^n}{\Gamma_n}}$. By using an M-averaged C_6 coefficient ($\approx$0.2 meV $\mu{\rm m}^6$) and the corresponding scaling to the probed crystal volume, we find that the simulated exciton numbers of $N_{\rm pump} = 500, \ldots, 3500$ (densities of

$\rho = 0.014, \ldots, 0.1\,\mu\text{m}^{-3}$ in a $10\times60\times60\,\mu\text{m}^3$ simulation volume) are mapped to laser powers of $P_{\text{pump}} = 2, \ldots, 20\,\mu\text{W}$. Already for those low powers, the saturation of the blockade effect has been observed experimentally [18], in agreement with our simulation.

Furthermore, we use the connection between laser power and plasma density from previous works [16] (for above band gap excitation) to estimate the density of the pump-induced EHP. At the largest examined pump power (20 μW), it has been shown [16] that only excitons $n \gtrsim 19$ are bleached, even if all the laser power was converted into a nanoplasma.

APPENDIX B: TRANSFORMATION BETWEEN LABORATORY AND INTEREXCITONIC AXIS

In the experiments [18], orthogonal linear polarizations for pump and probe laser were chosen that are defined with respect to the propagation direction. Then again, with respect to the interexcitonic axes, the overall magnetic quantum number M is defined, which is conserved under dipole-dipole interaction and hence serves to label the two-exciton states [22] ϕ_M. To calculate the excitation probability for a ϕ_M state by means of the overlap O (see main text), one must express the input state $|nX, n'Y\rangle_{\text{lab}}$ in the molecular frame with the interexcitonic axis as the quantization axis (nX refers to an X-polarized probe laser at frequency ω_n and $n'Y$ to a Y-polarized pump laser). This is done by rotating the laser axis in the direction of the interexcitonic axis via the Wigner d matrix, which can be given as [23]

$$d(\theta) = \begin{bmatrix} \cos(\theta) & 0 & -\sin(\theta) \\ 0 & 1 & 0 \\ \sin(\theta) & 0 & \cos(\theta) \end{bmatrix}, \tag{B1}$$

where θ is the angle between the two axes. In our case, we assume further to have a fixed angle ($\sim 15^\circ$) between the axes of the pump and probe lasers which makes it necessary to use two rotations as well as the Wigner D matrix [38].

[1] M. Saffman, T. G. Walker, and K. Mølmer, Quantum information with Rydberg atoms, Rev. Mod. Phys. **82**, 2313 (2010).

[2] C. S. Adams, J. D. Pritchard, and J. P. Shaffer, Rydberg atom quantum technologies, J. Phys. B: At. Mol. Opt. Phys. **53**, 012002 (2019).

[3] T. Kazimierczuk, D. Fröhlich, S. Scheel, H. Stolz, and M. Bayer, Giant Rydberg excitons in the copper oxide Cu_2O, Nature (London) **514**, 343 (2014).

[4] F. Schweiner, J. Main, G. Wunner, and C. Uihlein, k-dependent exchange interaction of the 1s orthoexciton in Cu_2O, Phys. Rev. B **94**, 115201 (2016).

[5] S. A. Lynch, C. Hodges, S. Mandal, W. Langbein, R. P. Singh, L. A. P. Gallagher, J. D. Pritchett, D. Pizzey, J. P. Rogers, C. S. Adams *et al.*, Rydberg excitons in synthetic cuprous oxide Cu_2O, Phys. Rev. Mater. **5**, 084602 (2021).

[6] V. Walther and T. Pohl, Plasma-enhanced interaction and optical nonlinearities of Cu_2O Rydberg excitons, Phys. Rev. Lett. **125**, 097401 (2020).

[7] L. A. P. Gallagher, J. P. Rogers, J. D. Pritchett, R. A. Mistry, D. Pizzey, C. S. Adams, M. P. A. Jones, P. Grünwald, V. Walther, C. Hodges *et al.*, Microwave-optical coupling via Rydberg excitons in cuprous oxide, Phys. Rev. Res. **4**, 013031 (2022).

[8] S. Steinhauer, M. A. M. Versteegh, S. Gyger, A. W. Elshaari, B. Kunert, A. Mysyrowicz, and V. Zwiller, Rydberg excitons in Cu_2O microcrystals grown on a silicon platform, Commun. Mater. **1**, 11 (2020).

[9] P. Grünwald, M. Aßmann, J. Heckötter, D. Fröhlich, M. Bayer, H. Stolz, and S. Scheel, Signatures of quantum coherences in Rydberg excitons, Phys. Rev. Lett. **117**, 133003 (2016).

[10] J. Taylor, S. Goswami, V. Walther, M. Spanner, C. Simon, and K. Heshami, Simulation of many-body dynamics using Rydberg excitons, Quantum Sci. Technol. **7**, 035016 (2022).

[11] K. Orfanakis, S. K. Rajendran, V. Walther, T. Volz, T. Pohl, and H. Ohadi, Rydberg exciton-polaritons in a Cu_2O microcavity, Nat. Mater. **21**, 767 (2022).

[12] T. Wang, Z. Li, Y. Li, Z. Lu, S. Miao, Z. Lian, Y. Meng, M. Blei, T. Taniguchi, K. Watanabe *et al.*, Giant valley-polarized Rydberg excitons in monolayer WSe_2 revealed by magneto-photocurrent spectroscopy, Nano Lett. **20**, 7635 (2020).

[13] M. A. M. Versteegh, S. Steinhauer, J. Bajo, T. Lettner, A. Soro, A. Romanova, S. Gyger, L. Schweickert, A. Mysyrowicz, and V. Zwiller, Giant Rydberg excitons in Cu_2O probed by photoluminescence excitation spectroscopy, Phys. Rev. B **104**, 245206 (2021).

[14] F. Schweiner, J. Main, G. Wunner, and C. Uihlein, Even exciton series in Cu_2O, Phys. Rev. B **95**, 195201 (2017).

[15] S. O. Krüger and S. Scheel, Interseries transitions between Rydberg excitons in Cu_2O, Phys. Rev. B **100**, 085201 (2019).

[16] J. Heckötter, M. Freitag, D. Fröhlich, M. Aßmann, M. Bayer, P. Grünwald, F. Schöne, D. Semkat, H. Stolz, and S. Scheel, Rydberg excitons in the presence of an ultralow-density electron-hole plasma, Phys. Rev. Lett. **121**, 097401 (2018).

[17] M. Aßmann and M. Bayer, Semiconductor Rydberg physics, Adv. Quantum Technol. **3**, 1900134 (2020).

[18] J. Heckötter, V. Walther, S. Scheel, M. Bayer, T. Pohl, and M. Aßmann, Asymmetric Rydberg blockade of giant excitons in cuprous oxide, Nat. Commun. **12**, 3556 (2021), under a Creative Commons licence (https://creativecommons.org/licenses/by/4.0/).

[19] C. F. Klingshirn, *Semiconductor Optics* (Springer-Verlag, Berlin, 2012).

[20] J. T. Warren, K. E. O'Hara, and J. P. Wolfe, Two-body decay of thermalized excitons in Cu_2O, Phys. Rev. B **61**, 8215 (2000).

[21] N. Naka, I. Akimoto, M. Shirai, and K.-I. Kan'no, Time-resolved cyclotron resonance in cuprous oxide, Phys. Rev. B **85**, 035209 (2012).

[22] V. Walther, S. O. Krüger, S. Scheel, and T. Pohl, Interactions between Rydberg excitons in Cu_2O, Phys. Rev. B **98**, 165201 (2018).

[23] S. Weber, C. Tresp, H. Menke, A. Urvoy, O. Firstenberg, H. P. Büchler, and S. Hofferberth, Calculation of Rydberg interaction potentials, J. Phys. B: At. Mol. Opt. Phys. **50**, 133001 (2017).

[24] F. Schöne, S.-O. Krüger, P. Grünwald, H. Stolz, S. Scheel, M. Aßmann, J. Heckötter, J. Thewes, D. Fröhlich, and M. Bayer,

Deviations of the exciton level spectrum in Cu_2O from the hydrogen series, Phys. Rev. B **93**, 075203 (2016).

[25] M. D. Lukin, M. Fleischhauer, R. Cote, L. M. Duan, D. Jaksch, J. I. Cirac, and P. Zoller, Dipole blockade and quantum information processing in mesoscopic atomic ensembles, Phys. Rev. Lett. **87**, 037901 (2001).

[26] D. Ziemkiewicz, G. Czajkowski, K. Karpiński, and S. Zielińska-Raczyńska, Nonlinear optical properties and kerr nonlinearity of Rydberg excitons in Cu_2O quantum wells, Phys. Rev. B **106**, 085431 (2022).

[27] R. Gutiérrez, J. P. Garrahan, and I. Lesanovsky, Self-similar nonequilibrium dynamics of a many-body system with power-law interactions, Phys. Rev. E **92**, 062144 (2015).

[28] Y. Toyozawa, Interband effect of lattice vibrations in the exciton absorption spectra, J. Phys. Chem. Solids **25**, 59 (1964).

[29] R. J. Elliott, Intensity of optical absorption by excitons, Phys. Rev. **108**, 1384 (1957).

[30] S. O. Krüger, H. Stolz, and S. Scheel, Interaction of charged impurities and Rydberg excitons in cuprous oxide, Phys. Rev. B **101**, 235204 (2020).

[31] E. Wigner, *Group Theory: And Its Application to the Quantum Mechanics of Atomic Spectra* (Academic Press, New York, 1959), Vol. 5.

[32] D. Cano and J. Fortágh, Nonadditive potentials between three Rydberg atoms, Phys. Rev. A **86**, 043422 (2012).

[33] A. Browaeys and T. Lahaye, Many-body physics with individually controlled Rydberg atoms, Nat. Phys. **16**, 132 (2020).

[34] M. Combescot and O. Betbeder-Matibet, Effective bosonic Hamiltonian for excitons: A too naive concept, Europhys. Lett. **59**, 579 (2002).

[35] J. Thewes, J. Heckötter, T. Kazimierczuk, M. Aßmann, D. Fröhlich, M. Bayer, M. A. Semina, and M. M. Glazov, Observation of high angular momentum excitons in cuprous oxide, Phys. Rev. Lett. **115**, 027402 (2015).

[36] V. Walther, R. Johne, and T. Pohl, Giant optical nonlinearities from Rydberg excitons in semiconductor microcavities, Nat. Commun. **9**, 1309 (2018).

[37] J. P. Rogers, L. A. P. Gallagher, D. Pizzey, J. D. Pritchett, C. S. Adams, M. P. A. Jones, C. Hodges, W. Langbein, and S. A. Lynch, High-resolution nanosecond spectroscopy of even-parity Rydberg excitons in Cu_2O, Phys. Rev. B **105**, 115206 (2022).

[38] D. A. Varshalovich, A. N. Moskalev, and V. Kel'manovich Khersonskii, *Quantum Theory of Angular Momentum* (World Scientific, Singapore, 1988).